Numerical Simulation of Wave Loading on Static Offshore Structures

Hrvoje Jasak, Vuko Vukčević and Inno Gatin

1 Introduction

The design of offshore structures requires information about peak loads that might occur during their service. The safety margin depends on the reliability of methods used to calculate these loads: smaller safety factors result in lower production and operational cost of structures. In order to acquire more precise information about wave loads, Computational Fluid Dynamic (CFD) methods are getting more attention. In [4], [5] active wave generation and absorption is described with moving boundaries and tested on various cases relevant to coastal engineering. On the other hand, [9] used the Spectral Wave Explicit Navier-Stokes Equations (SWENSE) method to calculate the forces on a buoy in both regular and irregular seas.

In this work, the Finite Volume Method (FVM) is used to calculate wave loads on static cylindrical structures. Such structures are often used as mounting points for offshore wind turbines (such as Tension Leg Platforms (TLP) and Spar Platforms). The phenomenon of freak wave is especially dangerous for offshore structures and the calculation of freak wave loads is a challenging task using conventional methods. One such calculation is presented here.

This chapter is organized as follows. In section 2 governing equations for two-phase flows are briefly described. Wave modelling using relaxation zones and its

Hrvoje Jasak
Wikki Ltd, 459 Southbank House, SE1 7SJ, London, United Kingdom, e-mail: h.jasak@wikki.co.uk,
Faculty of Mechanical Engineering and Naval Architecture - University of Zagreb, Ivana Lučića 5, 10000 Zagreb, Croatia, e-mail: hrvoje.jasak@fsb.hr

Vuko Vukčević
Faculty of Mechanical Engineering and Naval Architecture - University of Zagreb, Ivana Lučića 5, 10000 Zagreb, Croatia, e-mail: vuko.vukcevic@fsb.hr

Inno Gatin
Faculty of Mechanical Engineering and Naval Architecture - University of Zagreb, Ivana Lučića 5, 10000 Zagreb, Croatia, e-mail: innogatin@gmail.com

implicit treatment is the focal point of this section. In section 3 some details of the numerical procedure are given. In section 4, considered test cases are presented. Finally, a short conclusion is given, discussing the results of simulations and future work.

2 Mathematical Model

The mathematical model of incompressible, two-phase flow is presented in this section. Introducing the Volume-Of-Fluid (VOF) method for interface capturing [12] allows formulation of single continuity and momentum equation for mixture of phases. Furthermore, wave modelling using relaxation zones [6] is described. Finally, implicit blending technique is presented, where the CFD solution is forced to correspond to the potential flow solution within governing equations in order to efficiently generate and absorb waves.

2.1 Continuity and Momentum Equations

Numerical simulations are based on continuity (1) and mixture momentum equation (2). For viscid, incompressible and Newtonian fluid within mixture model, the volumetric continuity equation can be written as:

$$\nabla \bullet \mathbf{u} = 0\,, \tag{1}$$

and the mixture momentum equation reads:

$$\frac{\partial(\rho\mathbf{u})}{\partial t} + \nabla \bullet (\rho\mathbf{u}\mathbf{u}) = -\nabla p_d + \nabla \bullet (\mu\nabla\mathbf{u}) + \nabla\mathbf{u} \bullet \nabla\mu - \mathbf{f} \bullet \mathbf{x}\nabla\rho + \sigma\kappa\nabla\alpha\,. \tag{2}$$

Here, $\mathbf{u}$ is the velocity field, p_d is the dynamic pressure from $p = p_d + \rho\mathbf{g} \bullet \mathbf{x}$ decomposition. α is the volume fraction. Gravitational force is denoted with $\mathbf{f}$. According to [2], the last term models the surface tension effects. Furthermore, ρ and μ present density and dynamic viscosity, respectively. For more details on the derivation of the above equation, reader is referred to [11].

2.2 Volume of Fluid equation

The method is based on α indicator scalar field which is defined as:

$$\alpha(\mathbf{x}) = \begin{cases} 1\,, & \text{if } \mathbf{x} \in \Omega_1\,, \\ 0 < \alpha < 1\,, & \text{if } \mathbf{x} \text{ in the transitional area}\,, \\ 0\,, & \text{if } \mathbf{x} \in \Omega_2\,. \end{cases} \tag{3}$$

Ω_1 is the part of the domain occupied by the first phase (water), while Ω_2 is the part of the domain that contains the second phase (air). Cells that contain the free surface have the value of α between 0 and 1. Hence, α represents the ratio of the volume of first phase in given cell (V_1) and the total volume of the cell (V):

$$\alpha = \frac{V_1}{V}\,. \tag{4}$$

Fluid properties need to be defined before the solution of momentum equation, and are obtained using α:

$$\begin{aligned} \rho &= \alpha\rho_1 + (1-\alpha)\rho_2\,, \\ \mu &= \alpha\mu_1 + (1-\alpha)\mu_2\,. \end{aligned} \tag{5}$$

The transport equation for α is derived from phase continuity equation and reads:

$$\frac{\partial\alpha}{\partial t} + \nabla\bullet(\mathbf{u}\alpha) + \nabla\bullet(\mathbf{u}^r\alpha(1-\alpha)) = 0\,, \tag{6}$$

where the last term is responsible for interface compression as described in [10]. Novel formulation of compressive flux, $\mathbf{u}^r$ is given in next section.

2.3 Wave Modelling using Relaxation Zones

In CFD simulations, it is necessary to introduce incoming waves which do not arise naturally from governing equations. Since it is practically difficult to impose wave conditions on boundaries that will correspond to the given sea state, we shall introduce the concept of relaxation zones [6]. In such zones, wave modelling is conducted with coupling of potential flow wave theories and CFD solutions. They are used to smooth out the transition between wave theory and CFD solution, Figure 1. The inlet relaxation zone is used to generate incoming waves while the outlet relaxation zone to damp out outgoing waves without reflection, preventing the pollution of CFD results. The idea of relaxation zone is to volumetrically combine the governing equations, with solutions of simplified wave theory equations. Since wave theories are derived from Navier-Stokes equations, their solution shall be consistent with the governing laws and thus be available for blending. It is however necessary to account for simplifications in wave theory solutions in a consistent manner through the implicit blending procedure. The procedure is explained with general transport equation for variable ϕ:

$$\frac{\partial(\rho\phi)}{\partial t} + \nabla\bullet(\rho\mathbf{u}\phi) - \nabla\bullet(\gamma_\phi\nabla\phi) - S_u + S_p\phi = \mathcal{T}(\phi) = 0\,, \tag{7}$$

where γ_ϕ is the diffusion coefficient, S_u the source term and $S_p\phi$ linearised sink term. $\mathcal{T}(\phi)$ denotes general transport operator for future brevity. Now, consider that the $\phi_t(\mathbf{x},t)$ is the known, target solution obtained with different mathematical model (e.g. potential flow wave theory). Then, following equation can be written on boundaries:

$$\phi = \phi_t \rightarrow \phi - \phi_t = \mathcal{R}(\phi) = 0\,. \tag{8}$$

In the above equation, $\mathcal{R}(\phi)$ is the relaxation zone operator. Weight field, w is used to blend two models represented by equations (7) and (8). w is equal to 1 at the boundaries (inlet and outlet, cf. Figure 1), forcing the target solution. Toward the domain interior, w changes smoothly to 0 in order to force the full CFD solution. Finally, single equation can be written in terms of w and equations (7) and (8):

$$(1-w)\mathcal{T}(\phi) + w\mathcal{R}(\phi) = 0\,, \tag{9}$$

This will force the target solution given by equation (8) where $w = 1$, and give the full CFD solution (7) where $w = 0$. w is most often chosen to be the exponential function of the following form [6]:

$$w = \frac{\exp\left(\frac{d}{\lambda}\right)^p - 1}{\mathrm{e} - 1}\,, \tag{10}$$

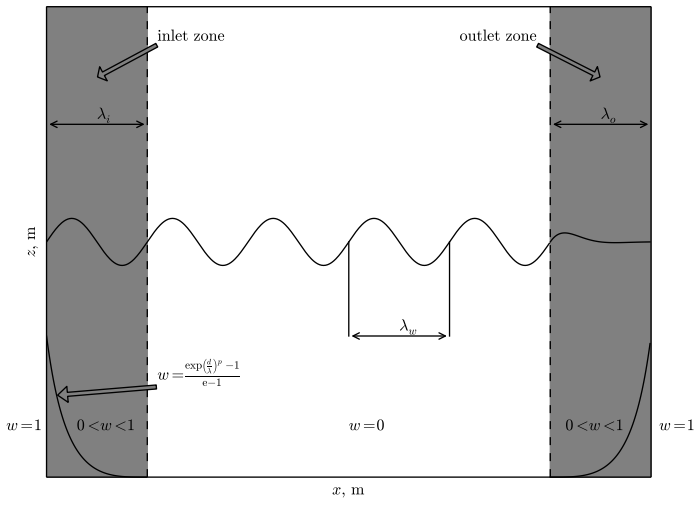

Fig. 1: Relaxation zones with weight field.

where d represents shortest distance to the boundary and λ the length of relaxation zone. p is the spatial exponent, usually set to 3.5. It should be noted that the length of the outlet relaxation zone should be approximately equal to wave length in order to prevent any wave reflection. In this approach, velocity field and volume fraction are blended in this manner, while the dynamic pressure equation is derived from continuity equation in the usual manner [7].

3 Numerical Model

Governing equations presented in the previous section 2 are implemented in OpenFOAM `Naval Hydro` pack. Pressure-velocity coupling is resolved with the PIMPLE algorithm that uses a few PISO correctors within each SIMPLE corrector. This treatment allows a number of successive solutions of VOF equation (6) in each time step in order to properly couple the density with velocity and pressure. Every equation is treated implicitly, including the VOF transport equation. Such procedure with implicit blending using relaxation zones allows stable simulations at maximum Courant-Friedrichs-Lewy (CFL) numbers higher than 1. The compressive flux needed for FVM discretization in equation (6) is defined as follows:

$$\mathbf{u}^r \bullet \mathbf{S} = c_\alpha \hat{n}_\Gamma \min\left(\frac{CFL_{ref}\Delta x}{\Delta t}, \frac{\mathbf{u} \bullet \mathbf{S}}{|\mathbf{S}|}\right), \tag{11}$$

where c_α represents the compression constant usually taken as 1, $\hat{n}_\Gamma$ is the free surface normal vector that has the magnitude of surface area. $CFL_{ref} = 0.5$ is the reference compression CFL number and Δx denotes the distance between cell centres encompassing the face. This formulation makes the compressive flux independent of the physical flux through free surface.

Linear upwind scheme is used for momentum convection while the van Leer, Total Variation Diminishing (TVD) scheme [13] is used for volume fraction convection. For compressive convection term, special `vofCompression` scheme is used which smoothly switches from central differencing in regions where $\alpha \approx 0.5$ to upwind differencing where $\alpha \approx 1$ or $\alpha \approx 0$. Hence, second order accuracy in space is achieved.

4 Test Cases

Two types of simulations are carried out with this model. The first simulation is used to validate the accuracy of the numerical simulation for regular waves. Wave loads on vertical cylinder are calculated and results are compared with experimental data from [1]. The second case shows the possibility of freak wave simulations.

4.1 Harmonic wave loads on vertical cylinder

The results of CFD simulations of wave loads on vertical cylinder are presented for five different incoming waves. The experimental measurements are carried out in a tank 36.5 m long, 2.4 m wide and 1.5 m deep. Circular cylinder is vertically immersed in water to the depth of 0.27 m; it does not reach the bottom of the tank. Cylinder diameter is 89 mm, and it is placed at 13.7 m from the wave maker. At the opposite end of the tank from the wave marker, a sloping beach is placed for wave absorption. There is enough room between the cylinder and the beach for the force measurements to be carried out before the reflected waves reach the cylinder, polluting the results. In [1] maximum measured forces in the longitudinal direction are given. Maximum values are determined over ten wave periods for each wave. The measurements are carried out for wave frequencies of 1.43, 1.1, 1.0, 0.9 and 0.7 Hz. For each frequency ten wave slopes ranging from 0.06 to 0.24 are used, where $k\eta_a$ is the wave slope, k wave number and η wave amplitude according to first order Stokes wave theory. Five waves are selected for numerical simulation and their parameters are presented in Table 1.

Table 1: Incident wave parameters.

Index N	Frequency f, hz	Wave slope $k\eta_a$, rad	Wave number k, rad/m	Wave height h, m	Wave length λ, m	Period T, s
1	0.70	0.06	1.97	0.060	3.19	1.43
2	0.70	0.12	1.97	0.120	3.19	1.43
3	0.90	0.20	3.26	0.123	1.93	1.11
4	1.10	0.12	4.87	0.050	1.30	0.90
5	1.43	0.20	8.83	0.049	0.76	0.70

The domain is reduced comparing to experimental setup to save computational time. Length of the domain is shortened to three wave lengths. The long tank is not needed since waves are absorbed completely in the outlet relaxation zone. Length of the inlet relaxation zone is set to half of the wave length, while the outlet relaxation zone is one wave length long. Smaller outlet relaxation zones proved to be reflective. Figure 2 shows the finite volume mesh in horizontal plane near the cylinder. Mesh used for calculations consists of 1 728 490 hexahedral cells. Maximum cell aspect ratio is 1:47. Linear grading is used to refine the mesh around the cylinder. As a result, cells near the cylinder are 140 times smaller that those near the boundaries.

Wave forces in longitudinal direction are obtained for each wave from Table 1. Figure 3 shows a representative force signal for the simulation of wave indexed by number 3. Table 2 presents the comparison of the results obtained by numerical simulation and experimental results for each wave. For waves 1,2 and 3 relative errors are within acceptable range. For higher frequencies the errors are larger. The accu-

racy of the calculation depends on the vertical mesh refinement, i.e. on the number of cells per wave height and on wave frequency. It can be seen in Table 2 that the error for wave 5 is significantly smaller when one uses finer mesh. It should be noted that finer mesh used for waves 4 and 5 is still relatively coarse mesh considering domain size, and it is believed that further refinement would improve the result. Furthermore, since waves 4 and 5 have smaller wave lengths (regarding to fixed distance between wave maker and the cylinder in experimental setup), non-linear effects should be more expressed at the time of the impact. Better results could probably be obtained with high order wave theories, but this was not investigated in the present study.

Table 2: Comparison of CFD and experimental results.

Wave index N	CFD results F_x, N	Experimental results F_x, N	Relative error Err, %	Number of cells	Courant number Co	α Courant number αCo
1	1.778	1.80	1.22	1 728 490	6.0	3.00
2	4.790	5.00	4.20	1 728 490	6.0	3.00
3	5.573	5.70	2.23	1 728 490	2.0	1.50
4	2.390	2.80	14.64	1 728 490	1.5	0.75
4	2.361	2.80	15.68	2 805 810	1.5	0.75
5	2.650	3.08	13.96	1 728 490	2.0	1.50
5	2.854	3.08	7.34	2 629 410	2.0	1.50

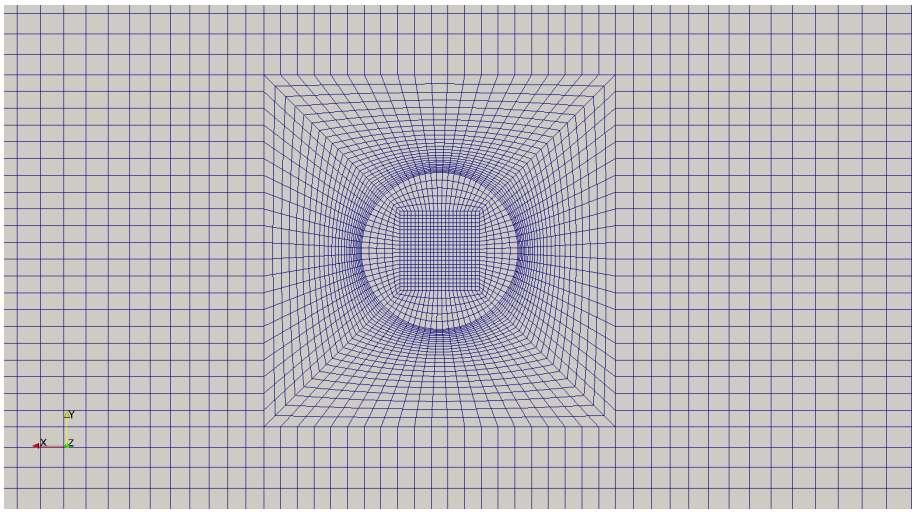

Fig. 2: Mesh geometry near the cylinder.

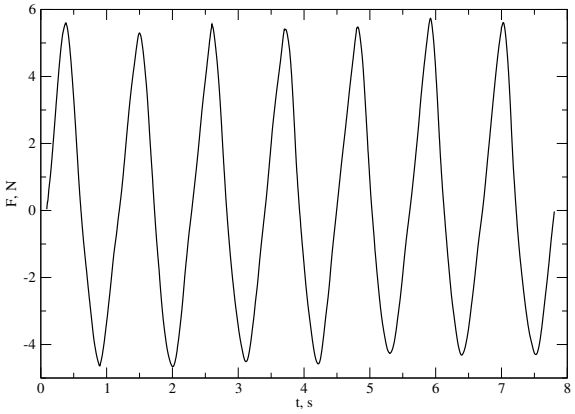

Fig. 3 Force signal for third wave (Table 1). Non-linear and higher order effects captured with CFD simulation can be seen as deviations from the regular sine wave in succesive load cycles presented in the figure. Local maximum values are constantly changing.

4.2 Freak wave simulation

Freak wave, also known as rouge wave, is a phenomenon that is not fully understood [8]. According to the definition that is most widely accepted, a freak wave is a wave whose height exceeds the significant wave height of the current sea state by two times [8]. Freak wave has a low probability of occurrence, but it poses a great threat to offshore structures and ships which is why new methods of calculating freak wave loads are getting more attention.

Harmonic wave focusing method is used to generate the freak wave. Harmonic waves used for focusing are components of Pierson-Moskowitz sea spectrum. This is done in order to obtain a more realistic freak wave, since sea spectrum describes realistic sea states. Free surface elevation is determined by superimposing individual harmonics. For this simulation, 30 wave components are used, guided by recommendation in [15]. Phase shifts of wave components are usually selected from a uniformly distributed random numbers. This ensures that the reproduced sea state is statistically equal to the sea state on which the wave energy spectrum is determined. However, to initialize a freak wave, phase angles must be set in a way that will ensure positive superposition of the wave components in order to achieve extreme wave height at desired time and position. Thus phase shifts are obtained by an optimization procedure. Freak wave in this study is obtained by linear superposition of wave components and is 0.255 m high, which is 2.12 times higher than selected significant wave height of 0.12 m.

Figure 4a depicts the freak wave profile in the simulation shortly before the focusing time of 2.66 s. Blue colour shows the part of the domain which contains water ($\alpha = 1$), while red colour shows the air in the domain ($\alpha = 0$). Thick horizontal white line in Figure 4a is positioned at calm free surface level. Thinner white horizontal lines show positive and negative significant amplitudes, i.e. distance between them is the significant wave height. Black horizontal lines are positioned at the crest and trough of the freak wave. Height difference is obvious, and it agrees well with the calculated height. White vertical line shows the position of the cylinders cen-

treline. Figure 4b shows a perspective view of the simulation at the same instant of time as in Figure 4a. Propagation of the freak wave caused further steepening. Figure 5a presents the freak wave impact on the circular cylinder. It can be observed that the wave was close to vertical at the time of impact. This is in accordance with often encountered description of freak wave as a ”wall of water”. Figure 5b presents excessive force caused by the freak wave at the time of the impact.

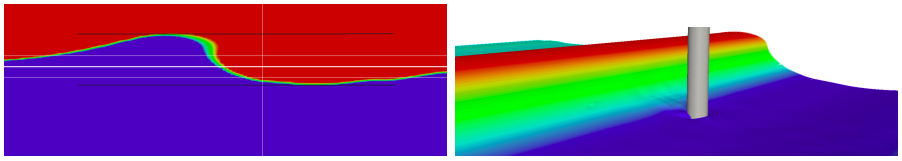

(a) Profile view. (b) Perspective view.

Fig. 4: Freak wave at the time instant before the wave impact.

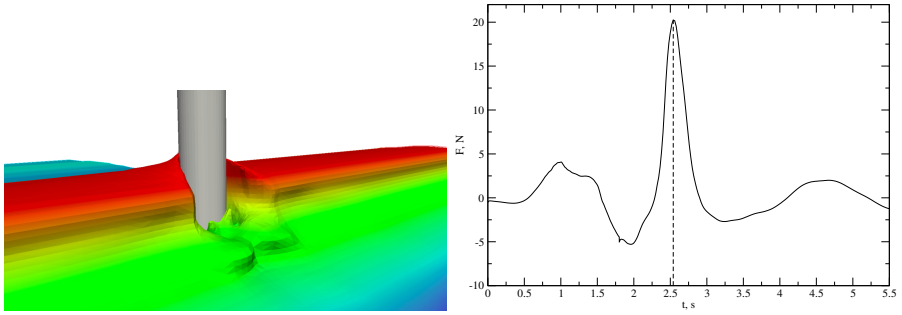

(a) Perspective view at the impact. (b) Longitudinal force exerted by the freak wave.

Fig. 5: Freak wave impact.

5 Conclusion and Future Work

This chapter described two-phase, incompressible CFD flow model specialized for offshore applications. Coupling with potential flow wave theories is obtained with implicit relaxation zones in second-order accurate FVM.

Numerical simulations of two types of problems are carried out which have practical application in modern offshore industry. The first case regarding regular wave loads agrees well with experimental results. The second case presents the possibility of evaluating loads on offshore structures and ships exerted by the freak wave,

which is hardly achievable using other, conventional methods. The results show that numerical simulations in OpenFOAM may indeed be used in the design process of offshore structures. Considerable savings could be made by using CFD results to get more detailed insight in the governing physics, gradually leading to a lower number of experiments.

Focal point of the future work will be further development of Spectral Wave Explicit Navier-Stokes Equations (SWENSE) method implemented in Finite Volume framework. Transition from the VOF to the implicitly redistanced Level Set interface capturing approach has been made. This allows efficient coupling of CFD near the structure of interest with arbitrary potential flow solutions in far field. Furthermore, the group will try to implement the Higher Order Spectrum (HOS) method [14], [3] in order to improve the freak wave simulations.

References

1. S. Y. Boo. Measurments of higher harmonic wave forces on a vertical truncated circular cylinder. *Ocean Engineering*, 33:219–233, 2006.
2. J.U. Brackbill, D.B. Kothe, and C. Zemach. A continuum method for modelling surface tension. *J. Comput. Phys.*, 100:335–354, 1992.
3. D. G. Dommermuth and D. K. P. Yue. A high-order spectral method for the study of nonlinear gravity waves. *J. Fluid. Mech.*, 184:267–288, 1987.
4. P. Higuera, J.L. Lara, and I. J. Losada. Realistic wave generation and active wave absorption for Navier-Stokes models: Application to OpenFoam®. *Coastal Engineering*, 71:102–118, 2013.
5. P. Higuera, J.L. Lara, and I. J. Losada. Simulating coastal engineering processes with OpenFoam ®. *Coastal Engineering*, 71:119–134, 2013.
6. N. G. Jacobsen, D. R. Fuhrman, and J. Fredsøe. A wave generation toolbox for the open-source CFD library: OpenFoam®. *Int. J. Numerl. Meth. Fluids*, 70(9):1073–1088, 2012.
7. H. Jasak. *Error Analysis and Estimation for the Finite Volume Method with Applications to Fluid Flows*. PhD thesis, Imperial College of Science, Technology & Medicine, London, 1996.
8. C. Kharif and E. Pelinovksy. Physical mechanisms of the rogue wave phonemenon. *European Journal of Mechanics - B/Fluids*, 22:603–634, 2003.
9. C. Monroy, G. Ducrozet, A. Bonnefoy, A. Babarit, and P. Ferrant. RANS simulations of a CALM buoy in regular and irregular seas using the SWENSE method. *Proceedings of the Twentieth (2010) International Offshore and Polar Engineering Conference, Beijing, China*, June 20-25, 2010.
10. H. Rusche. *Computational Fluid Dynamics of Dispersed Two - Phase Flows at High Phase Fractions*. PhD thesis, Imperial College of Science, Technology & Medicine, London, 2002.
11. O. Ubbink. *Numerical prediction of two fluid systems with sharp interfaces*. PhD thesis, Imperial College of Science, Technology & Medicine, London, 1997.
12. O. Ubbink and R. I. Issa. A method for capturing sharp fluid interfaces on arbitrary meshes. *Journal of Computational Physics*, 153:26–50, 1999.
13. B. van Leer. Towards the ultimate conservative difference scheme. IV. A new approach to numerical convection. *Journal of Computational Physics*, 23:276–299, 1977.
14. B. J. West, K. A. Brueckner, and R. S. Janda. A New Numerical Method for Surface Hydrodynamics. *Journal of Geophysical Research*, 92(C11):11803–11824, 1987.
15. X. Zhao. Numerical simulation of extreme wave generation using VOF method. *Journal of Hydrodynamics*, 22:466–477, 2010.